



Along-fault pore-pressure evolution during a slow-slip event in Guerrero, Mexico

W.B. Frank ^{a,*}, N.M. Shapiro ^a, A.L. Husker ^b, V. Kostoglodov ^b, H.S. Bhat ^a, M. Campillo ^c

^a Institut de Physique du Globe de Paris, Paris Sorbonne Cité, CNRS, Paris, France

^b Instituto de Geofísica, Universidad Nacional Autónoma de México, México D.F., Mexico

^c Institut des Sciences de la Terre, Université Joseph Fourier, CNRS, Grenoble, France



ARTICLE INFO

Article history:

Received 31 October 2014

Received in revised form 26 December 2014

Accepted 29 December 2014

Available online 21 January 2015

Editor: P. Shearer

Keywords:

slow slip

pore-pressure

subduction

low-frequency earthquakes

ABSTRACT

Slow earthquakes are important constituents of the seismic cycle and are involved in the stress transfer between the viscously slipping portion of the plate interface and the seismogenic zone. Their occurrence is likely associated with the near-lithostatic pore pressure in the slow earthquake source region, where fluids might modify fault friction and whose presence is indicated by high ratios of compressional (P)-wave velocity to shear (S)-wave velocity observed at the interface between the subducting plate and the overlying crust. Here we compare two slow earthquake phenomena observed in the Guerrero region of the Mexican subduction zone: low-frequency earthquakes (LFEs) and a slow-slip event (SSE) recorded by GPS. We observe variations of the LFE occurrence rates over month-long time scales during a large SSE that we interpret as a manifestation of transient changes in the fault shear strength. We argue that these transient changes are caused by a pore pressure fluctuation that migrates updip along the subduction interface. This mechanism suggests that fluids do not only passively weaken the plate interface but also play an active role in slow earthquake source regions.

© 2015 Elsevier B.V. All rights reserved.

1. Introduction

Slow earthquakes (Beroza and Ide, 2011) are a family of transient phenomena that release tectonic stress along the deep roots of plate interfaces. They principally manifest as slow-slip events (SSEs) that produce deformation measurable at the Earth's surface (Dragert et al., 2001) and low-intensity seismic emission called non-volcanic or tectonic tremor (TT) (Obara, 2002). Despite significantly different event durations that vary from minutes for TT to months for SSEs, and consequently significantly different magnitudes, all slow earthquake family members are strongly temporally, and frequently spatially, linked (Rogers and Dragert, 2003; Shelly et al., 2007). The most classic example, episodic tremor and slip (Rogers and Dragert, 2003), shows a strong increase of seismic TT activity at the plate interface during aseismic SSEs. While slow earthquakes play an important role in the seismic cycle by transferring stress from the viscously slipping downdip portion of faults to the shallow seismogenic zone, the mechanisms involved in their generation remain poorly constrained.

Slow earthquakes occur outside of the seismogenic zone where the frictional regime at the plate interface transitions from a stick-

slip regime to stable-sliding (Liu and Rice, 2005; Segall et al., 2010). The two most simple mechanisms to explain the weakening of the plate interface and the transition to stable-sliding with increasing distance from the trench are increasing temperatures with depth and increased pore-pressure from fluids released through metamorphic dehydration. Recent studies (Shelly et al., 2006; Audet et al., 2009; Song et al., 2009; Kim et al., 2010; Audet and Bürgmann, 2014) have suggested that trapped fluids at the plate interface and the consequent high pore pressures are the most important factor in creating the weak plate interface necessary for slow earthquakes.

We focus here on low-frequency earthquakes (LFEs), which are the smallest member of the slow earthquake family both in magnitude and in duration and are most often observed within TT (Shelly et al., 2006, 2007; Ide et al., 2007a). Previous studies (Ide et al., 2007b; Frank et al., 2013; Royer and Bostock, 2014) have shown them to be generated by small shear instabilities located along the transition zone between stick-slip and stable-sliding friction regimes at the subduction interface. An important feature of LFEs is that they can be precisely characterized in time and space because of their short duration and their distinctive multiplet behavior, where each source broadcasts many events over time forming a so-called LFE family (Shelly et al., 2007). By stacking all the events from a single LFE family, it is possible to reconstruct wave-

* Corresponding author.

E-mail address: frank@ipgp.fr (W.B. Frank).

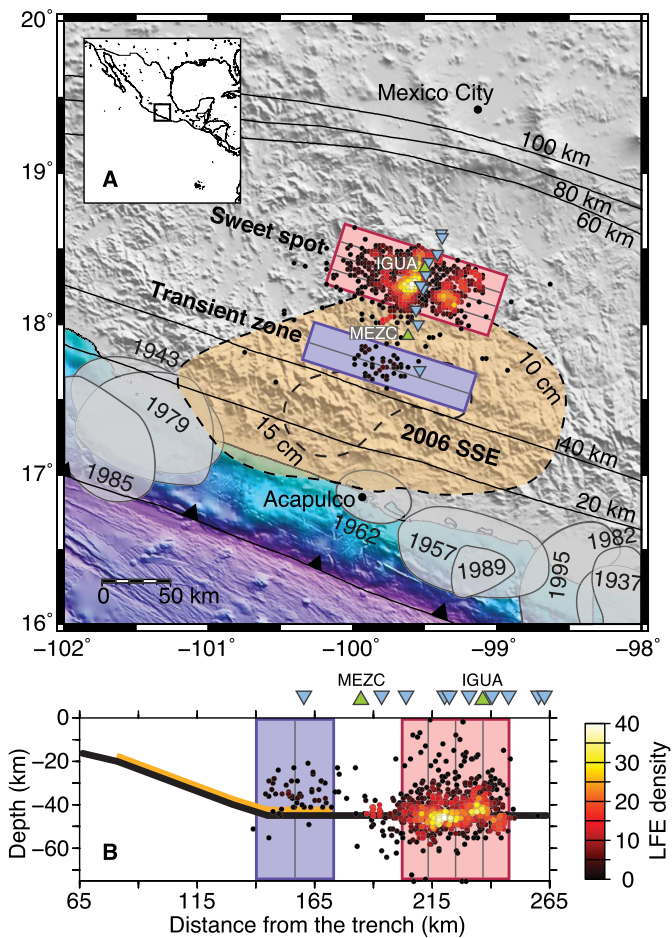


Fig. 1. Low-frequency earthquakes (LFEs) in Guerrero, Mexico. Each point represents an LFE source and family that is made up of thousands of multiplets; the color represents the number of other LFE sources less than 5 km away. The blue, inverted triangles represent the analyzed seismic network and the green triangles represent two local GPS stations. The geometry of the top of the subducting Cocos slab (Kim et al., 2013) is shown by the contours in A and the solid black line in B. The purple and red shaded areas respectively indicate the transient zone and the sweet spot (see text), and the thin gray lines within divide these LFE source regions into the analyzed subcatalogs. (A) The orange patch shows the region on the subduction interface that slipped during the 2006 SSE (Cavalié et al., 2013). The dashed contours show the amount of slip. The gray shaded patches indicate the rupture areas of megathrust earthquakes from the past 100 years and show that Guerrero slow earthquakes occur within a seismic gap. (B) The portion of the subduction interface that slipped during the 2006 SSE (15 cm contour in A) is indicated by the yellow stripe. (For interpretation of the references to color in this figure legend, the reader is referred to the web version of this article.)

forms with high signal-to-noise ratios that are used to accurately determine the family source location. With a precise location in time and space of LFE activity, one is able to closely monitor and therefore better understand, the response of the plate interface to large SSEs.

2. The Guerrero, Mexico LFE catalog

We study the LFE occurrence in Guerrero, Mexico (Fig. 1) where the flat subduction geometry (Pérez-Campos et al., 2008; Kim et al., 2010) results in a particularly favorable setting for the observation of slow earthquakes. Large magnitude and long duration SSEs are observed in Guerrero about every 4 yrs (Kostoglodov et al., 2010; Radiguet et al., 2012). We focus on one of these events that occurred between April 2006 and November 2006 using the Meso-America Subduction Experiment (MASE) dataset seismic network, which operated from 2005 to mid-2007 (Caltech, 2007). Previous studies of the MASE dataset showed extensive TT activity

that does not fully correlate in time and space with long-term SSEs (Kostoglodov et al., 2010; Husker et al., 2012). A majority of the TT occurred continuously in the “sweet spot” (Husker et al., 2012), located downdip of the SSE region and where LFEs have been more recently discovered (Frank et al., 2013).

We explore the Guerrero LFE catalog (Frank et al., 2014) generated via a systematic search that applied an automatic detection algorithm (Frank and Shapiro, 2014) to 2.5 yrs of continuous records from 10 MASE stations (Fig. 1). This catalog of unprecedented density contains more than 2000 events per day with a total of 1,849,486 LFEs regrouped into 1120 families. Because of the linear network geometry, the LFE location normal to the MASE network is not well constrained (Frank et al., 2013, 2014). We therefore only interpret event position along the network, which we represent as distance from the trench, d (Fig. 1B).

There is a strong difference in the LFE activity (Fig. 2) between the sweet spot and the region called the transient zone, which corresponds to the downdip part of the slab that slips during SSEs (Kostoglodov et al., 2010; Frank et al., 2014). In the transient zone, the LFEs are clearly grouped together in distinct bursts, whose frequency increases during the 2006 SSE. The bursts occur much more rapidly, however, in the sweet spot, demonstrated by the dense, sustained LFE activity that does not seem to be significantly affected by the SSE. Near continuous TT activity in Guerrero has also been reported (Husker et al., 2012) and corroborates similar observations in Japan (Obara et al., 2010) and Cascadia (Wech and Creager, 2011) where a clear reduction of TT recurrence with distance from the trench has been observed.

3. Fine-scale evolution of LFE activity

We first divide the dataset into subcatalogs based on the LFE sources' distance, d , from the trench (Fig. 1) to obtain a fine-scale representation of the processes that occur along the subduction interface. For each subcatalog, we calculate the cumulative number of LFEs as a function in time that is representative of the LFE energy release given their characteristic amplitude (Frank et al., 2014) and is shown in Fig. 3. Supposing that the period before the 2006 SSE represents an average inter-SSE activity trend, we calculate this trend separately for each subcatalog and then remove it to reveal the smaller scale activity variations that are hidden underneath. The normalized detrended cumulative counts shown in Fig. 4 characterize the LFE occurrence in the corresponding fault segments (Fig. 1). Because a slope of zero represents the inter-SSE LFE rate or trend, positive and negative slopes correspond respectively to accelerations and decelerations of LFE occurrence relative to the inter-SSE trend. We perform synthetic tests (described in Appendix A) to ensure that these trends are stable despite an inhomogeneous data coverage in time.

The most striking feature of Fig. 4 is the significant increase of LFE activity across both LFE source regions over two days that is synchronized with the GPS-observed 2006 SSE, similar to previous observations of increased TT activity in Guerrero (Kostoglodov et al., 2010; Husker et al., 2012). If we consider, however, the inter-SSE period before the slow slip, we observe distinct differences in activity between the sweet spot and the transient zone. Isolated steps corresponding to strong LFE bursts are clearly distinguishable in the subcatalogs located in the transient zone ($d < 175$ km), which we interpret as stick-slip-like behavior. Bursts of LFEs downdip in the sweet spot are, however, more frequent and their detrended cumulative count is more jagged, representing a more stable-sliding-like friction regime. The burst activity in the transient zone is synchronized with strong activity in the sweet spot, suggesting a rapid and long-range interaction such as elastic stress transfer.

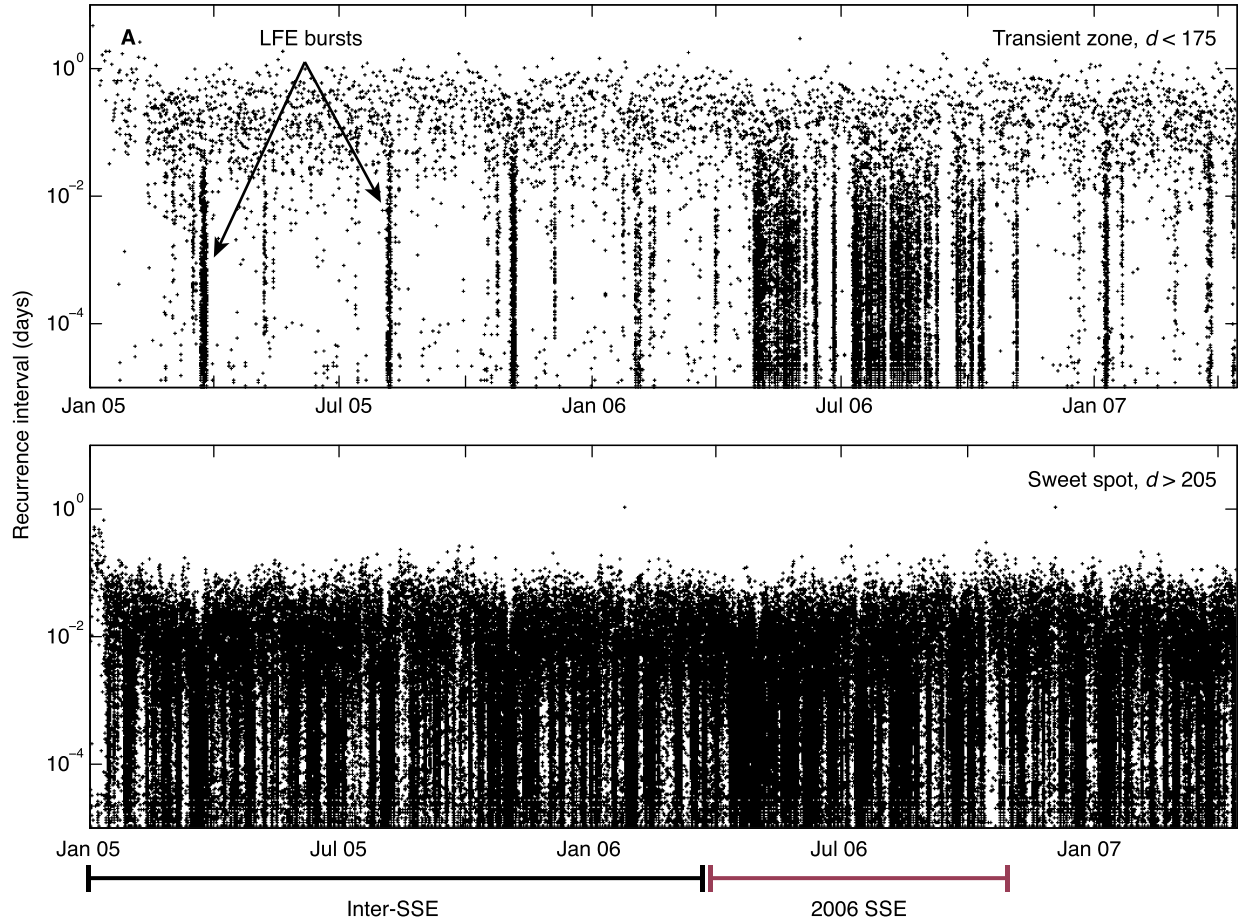


Fig. 2. Recurrence intervals of sequential LFEs within the transient zone (top) and the sweet spot (bottom), the two principal LFE source regions. The near-continuous activity in the sweet spot starkly contrasts the isolated LFE bursts in the transient zone during the inter-SSE period.

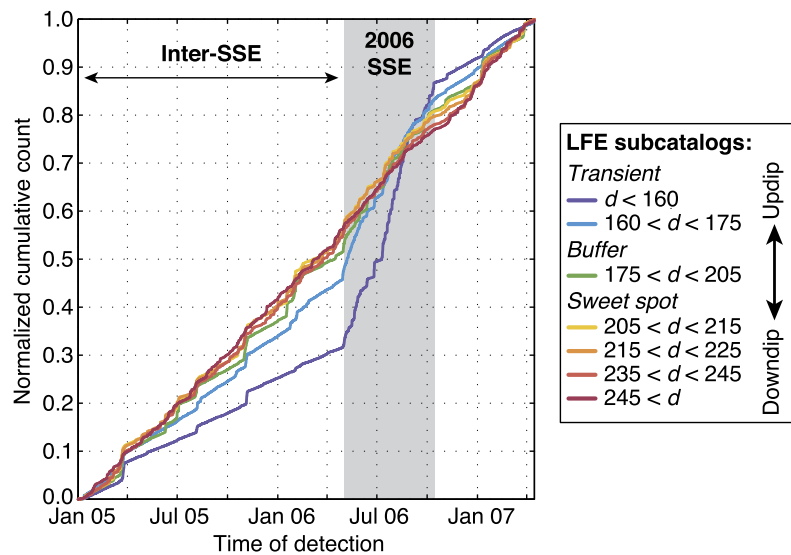


Fig. 3. Cumulative event count of the Guerrero LFE catalog. The cumulative counts of LFEs for different subcatalogs are shown by the colored lines. The LFE subcatalogs shown in Fig. 1 are sorted by their distance, d , from the trench. The inter-SSE trend drowns out all of the smaller scale activity variations, save the increase associated with the 2006 SSE (shown by the gray box) in the transient zone. (For interpretation of the references to color in this figure legend, the reader is referred to the web version of this article.)

An expected feature of the detrended LFE activity that commences during the 2006 SSE is a deceleration of activity that starts in mid-August 2006, a month and a half before the end of the slow-slip event, and lasts for about 4 months, ending well after

the 2006 SSE. This deceleration starts in the deepest portion of the sweet spot and then progressively extends updip over several weeks. After the deceleration, LFE activity then resumes its inter-SSE trend at the end of 2006.

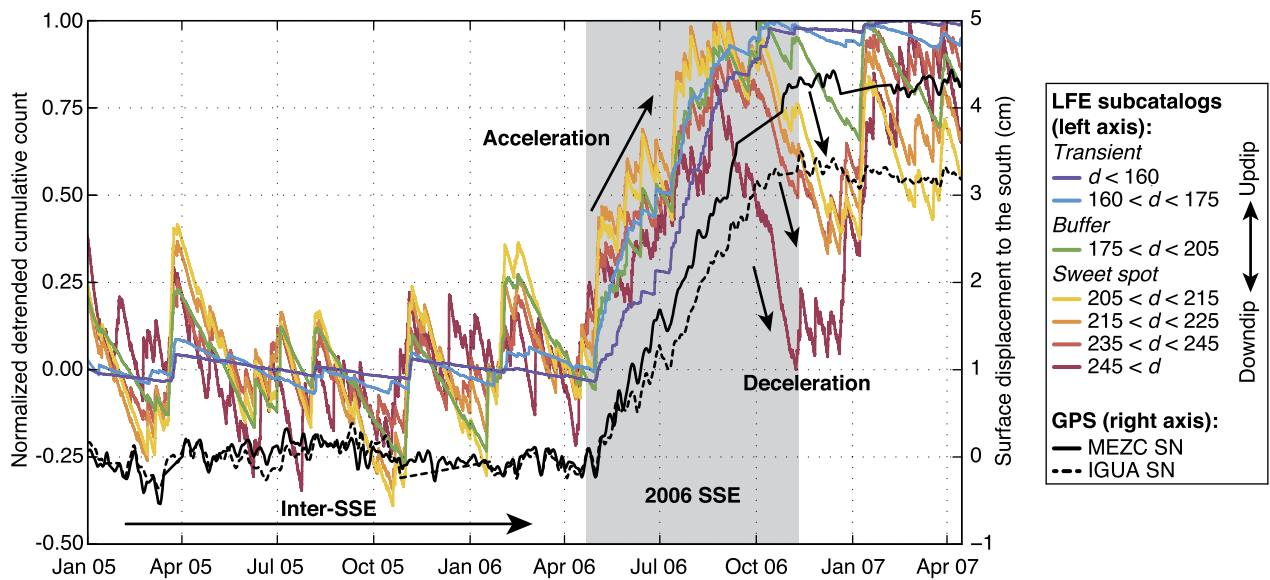


Fig. 4. LFE activity relative to inter-SSE trend. The cumulative counts of LFEs for different subcatalogs (Fig. 3) with the inter-SSE trend removed are shown by the colored lines. The LFE subcatalogs shown in Fig. 1 are sorted by their distance, d , from the trench. The detrended displacement measured by the two closest cGPS stations, shown in Fig. 1, are the solid and dashed black lines. The LFE activity goes through three different phases: (1) an inter-SSE trend; (2) an abrupt acceleration across the LFE source regions at the start of the SSE; (3) a progressive deceleration that starts in the sweet spot in the latter half of the SSE. (For interpretation of the references to color in this figure legend, the reader is referred to the web version of this article.)

4. Burst recurrence

The LFEs of the Guerrero catalog are organized primarily into bursts, both before and during the 2006 SSE (see Fig. 2 as well as Fig. 8 in Frank et al., 2014). We therefore apply a burst identification scheme to generate a catalog of LFE bursts for each of the fault segments (subcatalogs) and define their recurrence intervals (described in Appendix B). If we consider each burst of LFEs to represent a slip event, the length of their recurrence intervals can approximate whether each fault segment slips in a stick-slip (long recurrence) or a stable sliding (short recurrence) regime. Fig. 5 shows how the recurrence of LFE bursts varies as a function of distance from the trench. Before the start of the SSE in April 2006, we observe a progressive decrease of the recurrence interval with increasing distance from the trench; this is similar to what was reported in Cascadia (Wech and Creager, 2011) and Japan (Obara et al., 2010). We observe, however, a drastically different fault behavior during the 2006 SSE with LFE bursts occurring at the same rapid rate across the entire LFE source region, including the transient zone.

5. Discussion

If we consider each LFE source as a seismic asperity along the subduction interface, each repeated failure of that asperity represents an LFE multiplet. We can describe each multiplet as a Coulomb failure:

$$\sigma_s \geq \mu(\sigma_n - p), \quad (1)$$

where σ_s is shear stress, μ is the coefficient of friction, σ_n is the normal stress, and p is the pore pressure. We note that $\sigma_n - p$ is frequently referred to as the effective normal stress. We will now discuss in detail each of the three phases observed in the LFE activity evolution shown in Fig. 6.

5.1. Inter-SSE

Thermodynamic modeling of the Guerrero subduction zone predicts that fluids are released over time into the sweet spot

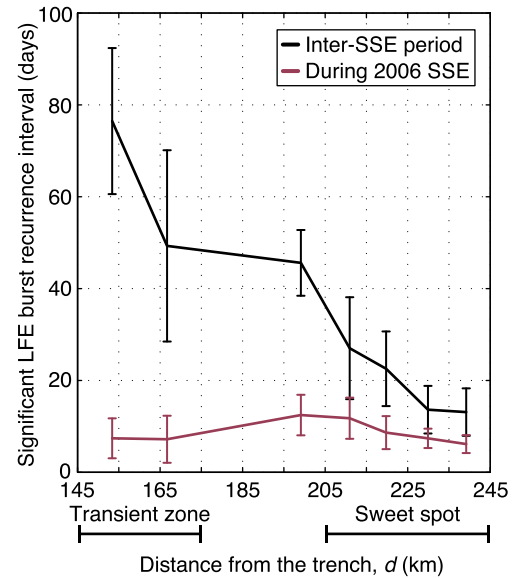


Fig. 5. Significant LFE burst recurrence intervals for before and during the 2006 SSE. The error bars are plotted as $\pm 1\sigma$. In contrast to the observed dependence of inter-SSE recurrence on distance from the trench (black), the entire source region exhibits a more stable-sliding-like behavior similar to the sweet spot during the 2006 SSE (red). We interpret this as the response of the plate interface to the increased shear stress due to the SSE. (For interpretation of the references to color in this figure legend, the reader is referred to the web version of this article.)

from the subducting oceanic crust by the metamorphic dehydration of metabasalt (Manea et al., 2004; Manea and Manea, 2011) (Fig. 6). Low-velocity layers with high V_p/V_s ratios have been observed in slow earthquake source regions (Audet et al., 2009; Song et al., 2009; Kim et al., 2010; Peacock et al., 2011). In Central Mexico, regional studies have suggested that the low-velocity layer is principally made up of serpentinites and talc (Kim et al., 2013) that develop strong layering parallel to the shearing axis, resulting in a strongly anisotropic permeability that discourages fault-perpendicular fluid flow (Mainprice et al., 2008; Kawano et al., 2011). We infer in absence of vertical fluid flow, the high pore-pressure at the plate interface is maintained and

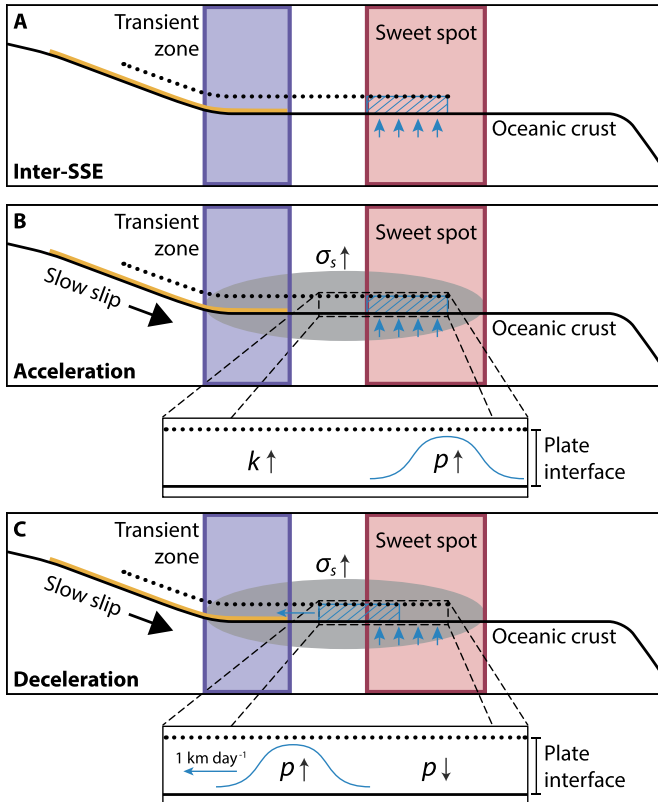


Fig. 6. Conceptual model of the evolution of LFE activity and pore pressure along the subduction interface during an SSE. The same features as Fig. 1B are shown along the vertical profile with the addition of the low-velocity zone (dotted line) (Song et al., 2009; Kim et al., 2010, 2013). The plate interface undergoes a three-phase evolution. Inter-SSE (A): high pore-pressure (hatched blue patch) in the sweet spot is maintained by the impermeable low-velocity zone trapping the fluids originating from the metamorphically dehydrating slab (Manea et al., 2004; Manea and Manea, 2011). Acceleration (B): strong shear slip due to the SSE increases the shear stress in the LFE source region, significantly increasing LFE activity. As the plate interface slips, an inter-connected network of reactivated fractures greatly increases the along-fault permeability, k . Deceleration (C): once the along-fault permeability is high enough (10^{-12} m^2), a sudden release of fluid pressure from the sweet spot starts to migrate up-dip along the interface. Following the passage of the high pressure pulse that travels at 1 km day^{-1} , the pore pressure, p , is reduced, increasing effective normal stress and decreasing LFE activity. (For interpretation of the references to color in this figure legend, the reader is referred to the web version of this article.)

the consequent low effective normal stress leads to the observed near continuous LFE activity in the sweet spot (Audet et al., 2009; Song et al., 2009; Kim et al., 2010; Peacock et al., 2011).

5.2. Acceleration

Once an SSE initiates, the slow slip that is concentrated up-dip of the two LFE source regions will slip faster relative to the LFE source regions and create a stress shadow downdip. The stress shadow will increase the stress, σ_s , in the LFE source regions and the left-hand side of Eq. (1). This will increase the rate of LFE failure and explains the abrupt increase of LFE activity observed in both the transient zone and the sweet spot in Fig. 4 and the reduction of burst recurrence intervals across the LFE source region seen in Fig. 5. Observations in Japan have drawn similar conclusions from seismicity rate increases within the overlying continental crust coincident with SSEs (Hirose et al., 2014; Fukuda et al., 2014).

Given that this acceleration mechanism would be due to slip up-dip of the two LFE source regions, the stress increase should diminish with increasing distance from the origin of the slip, or increasing distance from the trench. If we interpret the ratio of the

burst recurrence intervals during the SSE to the inter-SSE burst recurrence in Fig. 5 as the relative acceleration due to increased shear stress with respect to inter-SSE activity, the acceleration is much greater in the transient zone than in the sweet spot. This observation favors an acceleration mechanism up-dip of the source region such as the proposed stress shadow due to slow slip.

5.3. Deceleration

Increased stress in the LFE source region from the slow slip, however, can not be reconciled with the observed deceleration of LFE activity that starts in August 2006, three months into the SSE (Fig. 4). For LFE activity to decrease, the right-hand side of Eq. (1) must increase faster than the left-hand side. Seeing as the overlying crustal weight, σ_n , should not change, the two ways the right-hand side could experience a transient increase would be: (1) increasing μ or (2) decreasing p . Any potential mechanism must satisfy the observations: a constant value during the inter-SSE period, a delayed activation (increase of μ or decrease of p) during slow slip after three months of greatly increased LFE activity, and a rapid return to the inter-SSE value after the end of the SSE.

5.3.1. Possible mechanisms

Taking into account the observational conditions that must be satisfied, we do not favor the possibility of a transiently increasing friction. First, there is no simple mechanism, such as dilatancy (Segall et al., 2010), that would transiently increase the friction at an interface that is already slipping and in a perturbed state following the abrupt acceleration of LFE activity. A potential deceleration mechanism that would appeal to friction would be the decreasing slip rate or healing front of the slow slip. There are several discrepancies, however, with the observations. The first is that the deceleration is abrupt and occurs over a shorter timescale than the modeled decrease in slip rate that accompanies the healing front (Radiguet et al., 2011). If we consider the timing of the sweet spot deceleration in August 2006, the modeled source function of the 2006 SSE (Radiguet et al., 2011) places the peak slip rate more than a month before the first decelerating LFE subcatalog, making it unlikely that two observations are linked. Finally, after the first deceleration of LFE activity, there is still one more cm of slow slip observed at the IGUA cGPS station located directly above the deepest subcatalog. We find it difficult to reconcile ongoing slow slip with LFE activity at rates much slower than the inter-SSE trend, which is not associated with slow slip, and therefore do not suggest such a mechanism.

If we now compare the amplitude of the deceleration in the second half of the 2006 SSE to the smaller cyclic decelerations during the inter-SSE period for each of the LFE subcatalogs in Fig. 4, we observe that the amplitude of the deceleration increases with distance from the trench. A reduction in pore pressure would most likely have a greater effect in the sweet spot where near continuous LFE activity along with indirectly evidenced high pore pressures (Song et al., 2009; Kim et al., 2010) indicate a more lubricated or weakened plate interface compared to the brittle stick-slip regime in the transient zone. We therefore suggest that the observed space-time evolution of LFE activity requires a transient decrease in pore pressure at the plate interface during the second half of the SSE.

5.3.2. Up-dip migrating pore pressure pulse

During slow slip, the permeability structure in the localized shear zone of the subduction interface is significantly modified as previously healed fractures accommodate slip and are reactivated. The network of fractures becomes progressively more interconnected with an accumulation of accommodated slow slip, cre-

ating a temporary, localized region of high permeability, k , along the plate interface (Fig. 6C). To best describe this, we evoke the concept of a seismic valve or pump (Sibson, 1992). One could argue that SSEs do not rupture the subduction interface, so there wouldn't be any reactivation of dynamically ruptured fractures, but the existence of seismic slow earthquakes such as LFEs and tremor indicate that there is at least a portion of the slip that is accommodated dynamically.

Following an important increase of along-fault permeability over the first half of the SSE, the nearly lithostatic pore pressure in the sweet spot experiences a sudden release of pressure, emitting a pulse of high pore pressure that migrates updip along the interface (Rice, 1992). Given that the permeability of the fault interface is strongly dependent on pore pressure (Rice, 1992), the pore pressure pulse also transiently increases the permeability. Therefore, the pore pressure p behind the pulse is reduced relative to the pore pressure before the passage of the pulse. This increases the effective normal stress and decreasing LFE activity and explains the updip-migrating observed deceleration of activity. There should also be an increase of pore pressure before the deceleration as the pressure pulse travels along the interface and through each LFE subcatalog segment, consequently reducing the effective normal stress and increasing LFE activity; there is, however, no clear corresponding migratory increase of LFE activity. We suggest that this is due to the fact that the large and sudden acceleration observed at the beginning of the 2006 SSE attributed to increased shear stress dominates the increase of LFE activity and that any potential acceleration due to the pore pressure pulse is beneath the noise level of the detrended cumulative event count.

We observe the deceleration migrate from the deepest portion of the sweet spot to the transient zone over two months or so. Given the distance of ~ 70 km to be traveled, this suggests a pore pressure pulse velocity of about 1 km d^{-1} . We note that this propagation velocity is of the same order of magnitude as the 2006 SSE slip pulse (Radiguet et al., 2011). At the start of the LFE deceleration, however, the peak rate of the slip pulse is at least 100 km farther south than the first sweet spot subcatalog to slow down. At present it is difficult to rule whether the timing of the transient pore pressure evolution and the passage of the SSE slip pulse, both of which migrate at similar velocities, is coincidental or if there is a deeper link between the two observations.

5.3.3. Transient permeability along fault

We estimate the necessary permeability using the expression for the velocity of a pulse-like propagation of pore-pressure (Rice, 1992):

$$v = \frac{\gamma k}{\eta \phi}, \quad (2)$$

where v is the velocity of the propagating pore-pressure, γ is the specific weight difference between the fluid and the medium, k is the permeability, η is the viscosity of the fluid, and ϕ is the porosity. Using the observed migration velocity of 1 km d^{-1} , a specific weight difference of $1.6 \cdot 10^4 \text{ Pa m}^{-1}$ (using a serpentinite density of 2620 kg m^{-3}) (Reynard, 2013), a viscosity of 10^{-3} Pas (Miller et al., 2004), and a porosity of 0.05% (Kawano et al., 2011), we calculate a permeability of $3.6 \cdot 10^{-12} \text{ m}^2$.

We note that such a high permeability does not reflect the bulk permeability of the crust, but is restrained in space to the narrow localized shear zone of the plate interface and in time to the duration of the 2006 SSE. Similar transient permeabilities within fault zones have been observed in other geological contexts by measuring the migration velocity of fluid-induced seismic activity (Noir et al., 1997; Miller et al., 2004). Fluids might be also responsible for crustal velocity changes observed during SSEs in Guerrero (Rivet et al., 2011, 2014). Once the SSE finishes slipping, the seismic valve

then "closes" and the along-interface permeability is reduced to its original value following fault healing.

6. Conclusions

Our proposed scenario of the LFE response to the 2006 SSE occurs in three stages: (1) fluid released from metamorphic dehydration reactions is trapped within the sweet spot due to the strong anisotropic permeability of the low-velocity zone that is composed of serpentinite and talc (Song et al., 2009; Kim et al., 2010, 2013); (2) strong shear slip from the SSE increases the shear stress in the LFE source region, significantly increasing LFE activity; (3) slip at the plate interface creates an inter-connected network of reactivated faults that transiently increases along-fault permeability, causing a pulse of high pressure to travel from the sweet spot updip; pore pressure is reduced after the passage of fluid pressure pulse, increasing effective normal stress and decreasing LFE activity. This model explains both the increase of LFE activity during the 2006 SSE and the subsequent deceleration that migrates upwards along the subduction fault. Our findings suggest that fault pore-pressure can be rapidly and significantly modified in space and time, reflecting transient changes in permeability. Our model not only corroborates previous studies (Shelly et al., 2006; Audet et al., 2009; Peacock et al., 2011) arguing that fluid pore pressure is one of the most important physical parameters controlling fault strength, but also provides the first evidence of fluids' active role in the slow earthquake source region.

Acknowledgements

We thank Matthieu Landès for many insightful discussions concerning the burst detection method and the cumulative count error analysis. This work was supported by the Agence Nationale de la Recherche (France) under the contract RA0000CO69 (G-GAP) and by the European Research Council under the contract FP7 ERC Advanced Grant 227507 (WHISPER). N.M.S. was supported by the Russian Science Foundation (Grant 14-47-00002). Finally, one figure was made with Generic Mapping Tools (Wessel and Smith, 1998).

Appendix A. Error analysis

Fig. A.7 shows the number of functioning stations during the studied period. Given that our results are dependent on a constant rate of LFE detection, we analyzed the potential effect of station outages on the detrended cumulative count of an LFE catalog. We focus on the ten most populated LFE families from the subcatalog located in the sweet spot (darkest red subcatalog in Fig. 4). For these families, we generated a synthetic dataset with 100% uptime by concatenating the 422 days (out of 835 total) of the Guerrero dataset where all ten stations of the subnetwork used in the Guerrero LFE catalog functioned (Frank et al., 2014). We then computed a cumulative count of the control catalog from the 10 families that is represented by the red line in Fig. A.8.

In a next step we generated perturbed synthetic catalogs by introducing artificial station outages to the synthetic dataset. We first defined a time period of the synthetic dataset where station outages can start; we chose the time period to be the middle 30% of the synthetic dataset (between day 147 and day 275) so that each synthetic catalog would have a common component before and after the outages. For each synthetic catalog, we chose at random four stations (of ten total) that undergo three outages each. The start of each outage for each station is then generated individually as a uniformly distributed random day during the chosen outage time period; the duration of each outage for each station is a random number of days drawn from a normal distribution with a mean of 30 days and a standard deviation of 5 days.

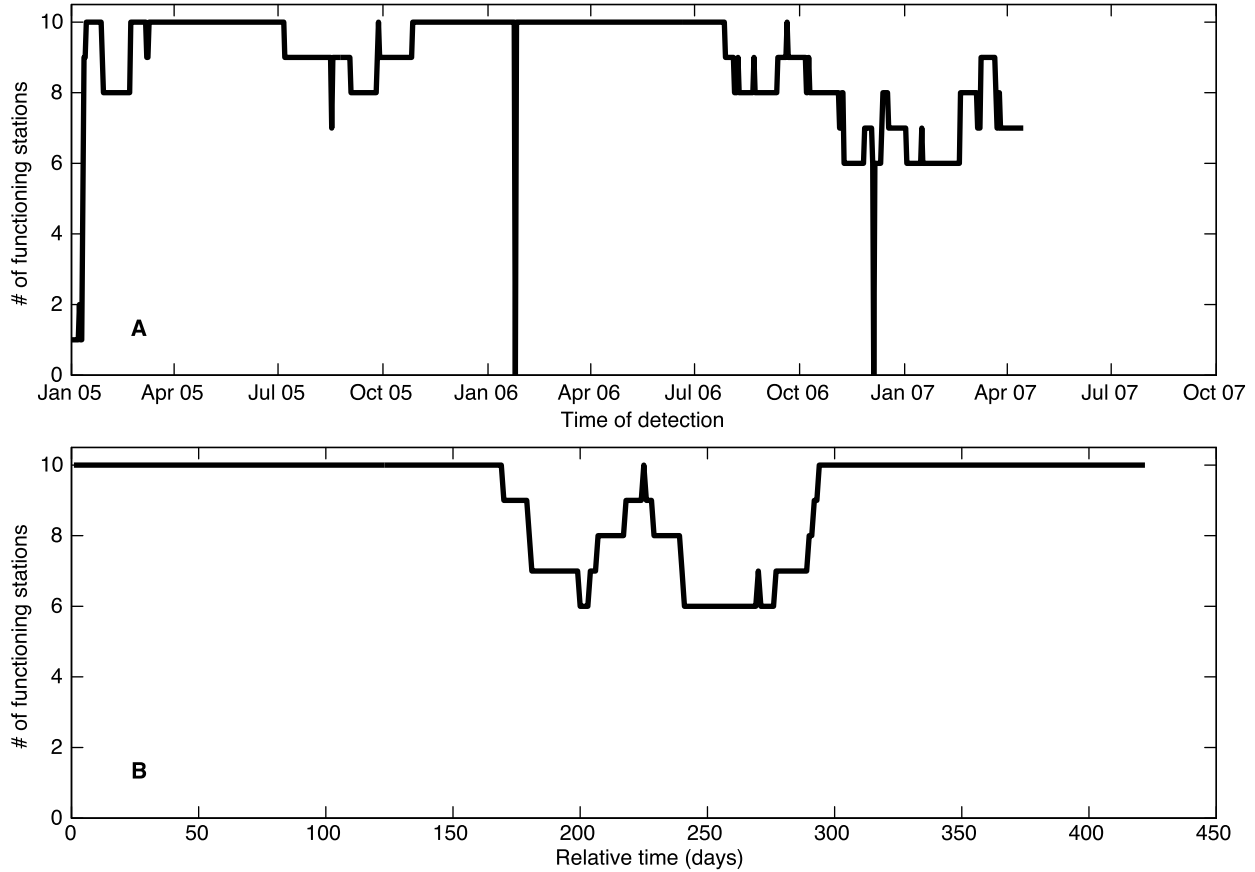


Fig. A.7. Station availability. (A) Actual station availability of the ten seismic stations used to generate the LFE catalog (Frank et al., 2014). (B) Example synthetic station outage.

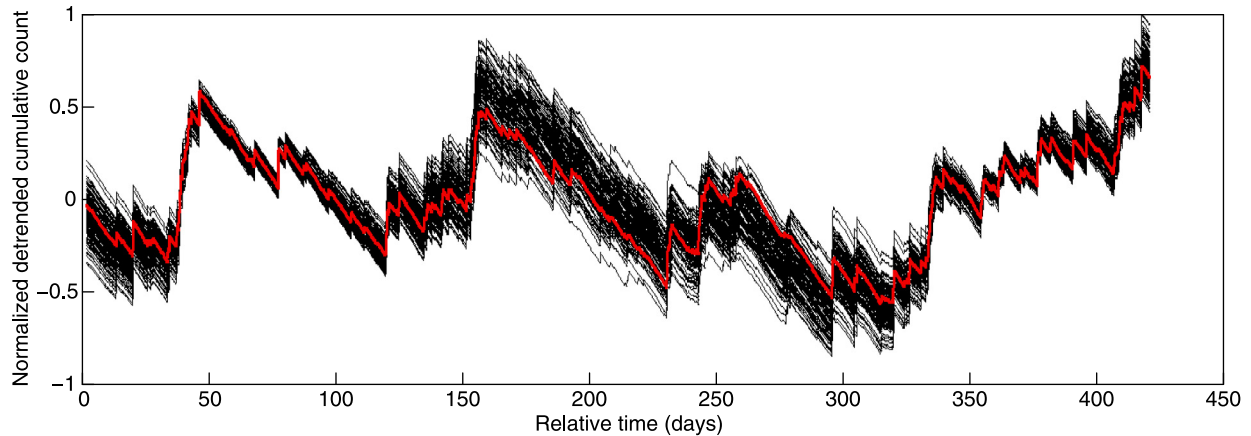


Fig. A.8. Detrended cumulative counts for the control and synthetic data. The control catalog (red line) is generated from the concatenated 422 days where all ten stations functioned. The 128 synthetic catalogs (black lines) are applied to the same dataset as the control catalog with imposed station outages in the middle 30% of the dataset. (For interpretation of the references to color in this figure legend, the reader is referred to the web version of this article.)

We then applied matched-filter searches using the same LFE families as in the control catalog, but first artificially removing the station data from the randomly generated outages. Each resulting synthetic catalog therefore underwent a different combination of station outages. We show an example of artificial station availability in Fig. A.7B. We show 128 synthetic catalogs generated using the method described above with black lines in Fig. A.8. Despite differences between the control catalog and the perturbed catalogs, most importantly, the same accelerations and decelerations in catalog activity are seen. For example, regardless of the different imposed station outages, all accelerations of LFE activity are

visible on every synthetic catalog, represented by a strong positive slope on the detrended cumulative count. Additionally, the size and duration of each acceleration and deceleration in LFE activity is extremely similar for each synthetic catalog relative to one another. This is demonstrated by the distribution of correlation coefficients calculated for the control catalog and each of the perturbed catalogs: the median correlation coefficient is 0.95 and minimum is 0.84. Even taking into the account the largest difference of 30% between the detrended control catalog and the synthetic catalogs, this extreme error does not come close to explaining the deceleration of LFE activity seen in Fig. 4. Given the results of this analysis,

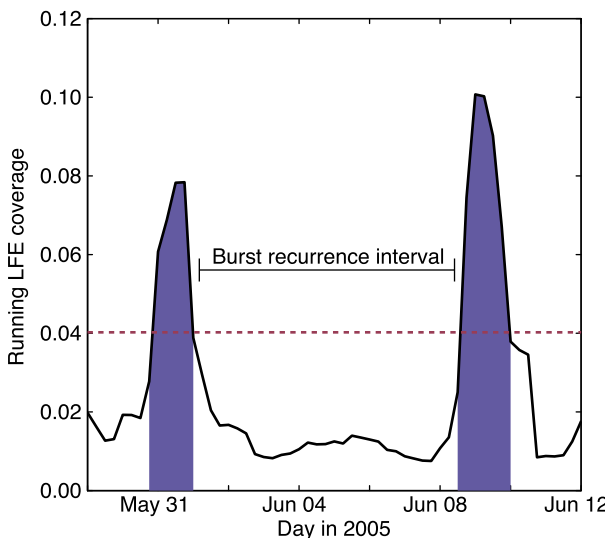


Fig. B.9. Two bursts detected within a sweet spot subcatalog. A threshold of two times the RMS (red dotted line) is used to detect two bursts (purple patches) from the running LFE coverage (black line). (For interpretation of the references to color in this figure legend, the reader is referred to the web version of this article.)

we assert that the principal results of this work are not affected by station outages.

Appendix B. Burst detection

The principal concept behind our burst detection method is that given a time window with a fixed-duration, we can estimate the activity of LFEs within that time window by calculating the time coverage of the LFE signals. Supposing some characteristic LFE signal duration d and a sampling rate Δt , we consider the detection time, τ_i , of the i th multiplet as the start of an LFE that lasts d seconds; therefore any time t between τ_i and $\tau_i + d$ is considered to be “covered” by an LFE. Based on previous observations of LFE durations in Mexico, we suppose a characteristic LFE duration d of 6 s (Frank et al., 2013). The LFE coverage, $C(T)$, of a time window centered at time T with a duration of L , is therefore defined as:

$$C(T) = \frac{\sum_{T-\frac{L}{2}}^{T+\frac{L}{2}} c(t)}{L \Delta t^{-1}}, \quad (\text{B.1})$$

where $c(t)$, the binary local coverage that contains every i th multiplet, is:

$$c(t) = \begin{cases} 1 & \text{if } \tau_i < t < \tau_i + d \\ 0 & \text{otherwise} \end{cases} \quad (\text{B.2})$$

With $c(t)$ defined in this way, we do not take into account multiple LFEs that slightly overlap each other: the greatest possible value of $c(t)$ is 1. The LFE coverage $C(T)$ can vary between 0 and 1: 0 when no LFEs are observed during the time window centered at T ; 1 when the entire time window centered at T is covered by LFEs. We then calculate the running coverage for the entire dataset using an L of one day, chosen to focus on the longer time-scale LFE activity.

Bursts of LFEs are determined by picking the time periods of the running LFE coverage that are over some threshold (Fig. B.9). We define the burst detection threshold for each catalog as two times the RMS of the running LFE coverage. The burst recurrence interval is then defined as the elapsed time between two sequential bursts. To only consider the inter-cluster recurrence intervals that represent the gross activity of each fault segment, we take into account the upper tritile ($>66\%$ quantile) of burst recurrence

intervals. The mean of the upper tritile that is plotted for each subcatalog in Fig. 5 is called the significant burst recurrence interval.

References

Audet, P., Bürgmann, R., 2014. Possible control of subduction zone slow-earthquake periodicity by silica enrichment. *Nature* 510, 389–392. <http://dx.doi.org/10.1038/nature13391>.

Audet, P., Bostock, M.G., Christensen, N.I., Peacock, S.M., 2009. Seismic evidence for overpressured subducted oceanic crust and megathrust fault sealing. *Nature* 457, 76–78. <http://dx.doi.org/10.1038/nature07650>.

Beroza, G.C., Ide, S., 2011. Slow earthquakes and nonvolcanic tremor. *Annu. Rev. Earth Planet. Sci.* 39, 271–296. <http://dx.doi.org/10.1146/annurev-earth-040809-152531>.

Caltech, 2007. Meso-America Subduction Experiment (MASE) dataset. <http://dx.doi.org/10.7909/C3RN35P>.

Cavalié, O., Pathier, E., Radiguet, M., Vergnolle, M., Cotte, N., Walpersdorf, A., Kostoglodov, V., Cotton, F., 2013. Slow slip event in the Mexican subduction zone: evidence of shallower slip in the Guerrero seismic gap for the 2006 event revealed by the joint inversion of InSAR and GPS data. *Earth Planet. Sci. Lett.* 367, 52–60. <http://dx.doi.org/10.1016/j.epsl.2013.02.020>.

Dragert, H., Wang, K., James, T.S., 2001. A silent slip event on the deeper Cascadia subduction interface. *Science* 292, 1525–1528. <http://dx.doi.org/10.1126/science.1060152>.

Frank, W.B., Shapiro, N.M., 2014. Automatic detection of low-frequency earthquakes (LFEs) based on a beamformed network response. *Geophys. J. Int.* 197 (2), 1215–1223. <http://dx.doi.org/10.1093/gji/ggu058>.

Frank, W.B., Shapiro, N.M., Kostoglodov, V., Husker, A.L., Campillo, M., Payero, J.S., Prieto, G.A., 2013. Low-frequency earthquakes in the Mexican sweet spot. *Geophys. Res. Lett.* 40, 2661–2666. <http://dx.doi.org/10.1002/grl.50561>.

Frank, W.B., Shapiro, N.M., Husker, A.L., Kostoglodov, V., Romanenko, A., Campillo, M., 2014. Using systematically characterized low-frequency earthquakes as a fault probe in Guerrero, Mexico. *J. Geophys. Res.* 119 (10), 1686–1700. <http://dx.doi.org/10.1002/2014JB011457>.

Fukuda, J., Kato, A., Obara, K., Miura, S., Kato, T., 2014. Imaging of the early acceleration phase of the 2013–2014 Boso slow slip event. *Geophys. Res. Lett.* 41 (21), 7493–7500. <http://dx.doi.org/10.1002/2014GL061550>.

Hirose, H., Matsuzawa, T., Kimura, T., 2014. The Boso slow slip events in 2007 and 2011 as a driving process for the accompanying earthquake swarm. *Geophys. Res. Lett.* 41 (8), 2778–2785. <http://dx.doi.org/10.1002/2014GL059791>.

Husker, A.L., Kostoglodov, V., Cruz-Atienza, V.M., Legrand, D., Shapiro, N.M., Payero, J.S., Campillo, M., Huesca-Pérez, E., 2012. Temporal variations of non-volcanic tremor (NVT) locations in the Mexican subduction zone: finding the NVT sweet spot. *Geochem. Geophys. Geosyst.* 13 (3), Q03011. <http://dx.doi.org/10.1029/2011GC003916>.

Ide, S., Beroza, G.C., Shelly, D.R., Uchide, T., 2007a. A scaling law for slow earthquakes. *Nature* 447, 76–79. <http://dx.doi.org/10.1038/nature05780>.

Ide, S., Shelly, D.R., Beroza, G.C., 2007b. Mechanism of deep low frequency earthquakes: further evidence that deep non-volcanic tremor is generated by shear slip on the plate interface. *Geophys. Res. Lett.* 34, L03308. <http://dx.doi.org/10.1029/2006GL028890>.

Kawano, S., Katayama, I., Okazaki, K., 2011. Permeability anisotropy of serpentinite and fluid pathways in a subduction zone. *Geology* 39 (10), 939–942. <http://dx.doi.org/10.1130/G32173.1>.

Kim, Y., Clayton, R.W., Jackson, J.M., 2010. Geometry and seismic properties of the subducting Cocos plate in central Mexico. *J. Geophys. Res.* 115, B06310. <http://dx.doi.org/10.1029/2009JB006942>.

Kim, Y., Clayton, R.W., Asimow, P.D., Jackson, J.M., 2013. Generation of talc in the mantle wedge and its role in subduction dynamics in central Mexico. *Earth Planet. Sci. Lett.* 384, 81–87. <http://dx.doi.org/10.1016/j.epsl.2013.10.006>.

Kostoglodov, V., Husker, A.L., Shapiro, N.M., Payero, J.S., Campillo, M., Cotte, N., Clayton, R.W., 2010. The 2006 slow slip event and nonvolcanic tremor in the Mexican subduction zone. *Geophys. Res. Lett.* 37, L24301. <http://dx.doi.org/10.1029/2010GL045424>.

Liu, Y., Rice, J.R., 2005. Aseismic slip transients emerge spontaneously in three-dimensional rate and state modeling of subduction earthquake sequences. *J. Geophys. Res.* 110, B08307. <http://dx.doi.org/10.1029/2004JB003424>.

Mainprice, D., Le Page, Y., Rodgers, J., Jouanna, P., 2008. Ab initio elastic properties of talc from 0 to 12 GPa: interpretation of seismic velocities at mantle pressures and prediction of auxetic behaviour at low pressure. *Earth Planet. Sci. Lett.* 274, 327–338. <http://dx.doi.org/10.1016/j.epsl.2008.07.047>.

Manea, V.C., Manea, M., 2011. Flat-slab thermal structure and evolution beneath Central Mexico. *Pure Appl. Geophys.* 168, 1475–1487. <http://dx.doi.org/10.1007/s00224-010-0207-9>.

Manea, V.C., Manea, M., Kostoglodov, V., Currie, C.A., Sewell, G., 2004. Thermal structure, coupling and metamorphism in the Mexican subduction zone beneath Guerrero. *Geophys. J. Int.* 158 (2), 775–784. <http://dx.doi.org/10.1111/j.1365-246X.2004.02325.x>.

Miller, S.A., Collettini, C., Chiaraluce, L., Cocco, M., Barchi, M., Kaus, B.J.P., 2004. Aftershocks driven by a high-pressure CO₂ source at depth. *Nature* 427, 724–727. <http://dx.doi.org/10.1038/nature02251>.

Noir, J., Jacques, E., Békri, S., Adler, P.M., Tapponnier, P., King, G.C.P., 1997. Fluid flow triggered migration of events in the 1989 Dobi Earthquake sequence of central Afar. *Geophys. Res. Lett.* 24 (18), 2335–2338. <http://dx.doi.org/10.1029/97GL02182>.

Obara, K., 2002. Nonvolcanic deep tremor associated with subduction in southwest Japan. *Science* 296, 1679–1681. <http://dx.doi.org/10.1126/science.1070378>.

Obara, K., Tanaka, S., Maeda, T., Matsuzawa, T., 2010. Depth-dependent activity of non-volcanic tremor in southwest Japan. *Geophys. Res. Lett.* 37, L13306. <http://dx.doi.org/10.1029/2010GL043679>.

Peacock, S.M., Christensen, N.I., Bostock, M.G., Audet, P., 2011. High pore pressures and porosity at 35 km depth in the Cascadia subduction zone. *Geology* 39 (5), 471–474. <http://dx.doi.org/10.1130/G31649.1>.

Pérez-Campos, X., Kim, Y., Husker, A.L., Davis, P.M., Clayton, R.W., Iglesias, A., Pacheco, J.F., Singh, S.K., Manea, V.C., Gurnis, M., 2008. Horizontal subduction and truncation of the Cocos Plate beneath central Mexico. *Geophys. Res. Lett.* 35, L18303. <http://dx.doi.org/10.1029/2008GL035127>.

Radiguet, M., Cotton, F., Vergnolle, M., Campillo, M., Valette, B., Kostoglodov, V., Cotte, N., 2011. Spatial and temporal evolution of a long term slow slip event: the 2006 Guerrero Slow Slip Event. *Geophys. J. Int.* 184 (2), 816–828. <http://dx.doi.org/10.1111/j.1365-246X.2010.04866.x>.

Radiguet, M., Cotton, F., Vergnolle, M., Campillo, M., Walpersdorf, A., Cotte, N., Kostoglodov, V., 2012. Slow slip events and strain accumulation in the Guerrero gap, Mexico. *J. Geophys. Res.* 117, B04305. <http://dx.doi.org/10.1029/2011JB008801>.

Reynard, B., 2013. Serpentine in active subduction zones. *Lithos* 178, 171–185. <http://dx.doi.org/10.1016/j.lithos.2012.10.012>.

Rice, J.R., 1992. Fault stress states, pore pressure distributions, and the weakness of the San Andreas fault. In: *Fault Mechanics and Transport Properties of Rocks*. Elsevier, pp. 475–503, Chapter 20.

Rivet, D., Campillo, M., Shapiro, N.M., Cruz-Atienza, V.M., Radiguet, M., Cotte, N., Kostoglodov, V., 2011. Seismic evidence of nonlinear crustal deformation during a large slow slip event in Mexico. *Geophys. Res. Lett.* 38, L08308. <http://dx.doi.org/10.1029/2011GL047151>.

Rivet, D., Campillo, M., Radiguet, M., Zigone, D., Cruz-Atienza, V.M., Shapiro, N.M., Kostoglodov, V., Cotte, N., Cougoulat, G., Walpersdorf, A., Daub, E.G., 2014. Seismic velocity changes, strain rate and non-volcanic tremors during the 2009–2010 slow slip event in Guerrero, Mexico. *Geophys. J. Int.* 196, 447–460. <http://dx.doi.org/10.1093/gji/gjt374>.

Rogers, G., Dragert, H., 2003. Episodic tremor and slip on the Cascadia subduction zone: the chatter of silent slip. *Science* 300, 1942–1943. <http://dx.doi.org/10.1126/science.1084783>.

Royer, A.A., Bostock, M.G., 2014. A comparative study of low frequency earthquake templates in northern Cascadia. *Earth Planet. Sci. Lett.* 402, 247–256. <http://dx.doi.org/10.1016/j.epsl.2013.08.040>.

Segall, P., Rubin, A.M., Bradley, A.M., Rice, J.R., 2010. Dilatant strengthening as a mechanism for slow slip events. *J. Geophys. Res.* 115, B12305. <http://dx.doi.org/10.1029/2010JB007449>.

Shelly, D.R., Beroza, G.C., Ide, S., Nakamura, S., 2006. Low-frequency earthquakes in Shikoku, Japan, and their relationship to episodic tremor and slip. *Nature* 442, 188–191. <http://dx.doi.org/10.1038/nature04931>.

Shelly, D.R., Beroza, G.C., Ide, S., 2007. Non-volcanic tremor and low-frequency earthquake swarms. *Nature* 446, 305–307. <http://dx.doi.org/10.1038/nature05666>.

Sibson, R.H., 1992. Implications of fault-valve behaviour for rupture nucleation and recurrence. *Tectonophysics* 211, 283–293.

Song, T.-R.A., Helmberger, D.V., Brudzinski, M.R., Clayton, R.W., Davis, P.M., Pérez-Campos, X., Singh, S.K., 2009. Subducting slab ultra-slow velocity layer coincident with silent earthquakes in southern Mexico. *Science* 324, 502–506. <http://dx.doi.org/10.1126/science.1167595>.

Wech, A.G., Creager, K.C., 2011. A continuum of stress, strength and slip in the Cascadia subduction zone. *Nat. Geosci.* 4, 624–628. <http://dx.doi.org/10.1038/ngeo1215>.

Wessel, P., Smith, W.H.F., 1998. New, improved version of generic mapping tools released. *Eos Trans. AGU* 79 (47), 579. <http://dx.doi.org/10.1029/98EO00426>.